Acta Pharmaceutica Sinica B 2020;10(7):1216–1227

Chinese Pharmaceutical Association
Institute of Materia Medica, Chinese Academy of Medical Sciences

Acta Pharmaceutica Sinica B

www.elsevier.com/locate/apsb
www.sciencedirect.com

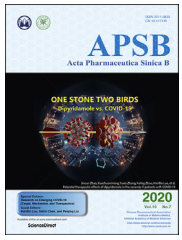

ORIGINAL ARTICLE

Dose selection of chloroquine phosphate for treatment of COVID-19 based on a physiologically based pharmacokinetic model

Cheng Cui[a], Miao Zhang[a], Xueting Yao[a], Siqi Tu[a], Zhe Hou[a], Valerie Sia Jie En[a], Xiaoqiang Xiang[b], Jing Lin[c], Ting Cai[c], Ning Shen[d], Chunli Song[e], Jie Qiao[f], Shun Zhang[c,*], Haiyan Li[a,g,*], Dongyang Liu[a,*]

[a]*Drug Clinical Trial Center, Peking University Third Hospital, Beijing 100191, China*
[b]*Department of Clinical Pharmacy, School of Pharmacy, Fudan University, Shanghai 201203, China*
[c]*Key Laboratory of Diagnosis and Treatment of Digestive System Tumors of Zhejiang Province, HwaMei Hospital, University of Chinese Academy of Sciences (Ningbo No.2 Hospital), Ningbo 315010, China*
[d]*Department of Respirator, Peking University Third Hospital, Beijing 100191, China*
[e]*Department of Orthopedics, Peking University Third Hospital, Beijing 100191, China*
[f]*Center for Reproductive Medicine, Department of Obstetrics and Gynecology, Peking University Third Hospital, Beijing 100191, China*
[g]*Department of Cardiology and Institute of Vascular Medicine, Peking University Third Hospital, Beijing 100191, China*

Received 17 March 2020; received in revised form 24 March 2020; accepted 25 March 2020

KEY WORDS

COVID-19;
Chloroquine phosphate;
PBPK;
Dosing strategy

Abstract Chloroquine (CQ) phosphate has been suggested to be clinically effective in the treatment of coronavirus disease 2019 (COVID-19). To develop a physiologically-based pharmacokinetic (PBPK) model for predicting tissue distribution of CQ and apply it to optimize dosage regimens, a PBPK model, with parameterization of drug distribution extrapolated from animal data, was developed to predict human tissue distribution of CQ. The physiological characteristics of time-dependent accumulation was mimicked through an active transport mechanism. Several dosing regimens were proposed based on PBPK simulation combined with known clinical exposure–response relationships. The model was also validated by clinical data from Chinese patients with COVID-19. The novel PBPK model allows in-depth description of the pharmacokinetics of CQ in several key organs (lung, heart, liver, and kidney),

*Corresponding authors.
E-mail addresses: liudongyang@vip.sina.com (Dongyang Liu), haiyanli1027@hotmail.com (Haiyan Li), zhangshun@ucas.ac.cn (Shun Zhang).
Peer review under responsibility of Chinese Pharmaceutical Association and Institute of Materia Medica, Chinese Academy of Medical Sciences.

https://doi.org/10.1016/j.apsb.2020.04.007

and was applied to design dosing strategies in patients with acute COVID-19 (Day 1: 750 mg BID, Days 2−5: 500 mg BID, CQ phosphate), patients with moderate COVID-19 (Day 1: 750 mg and 500 mg, Days 2−3: 500 mg BID, Days 4−5: 250 mg BID, CQ phosphate), and other vulnerable populations (*e.g.*, renal and hepatic impairment and elderly patients, Days 1−5: 250 mg BID, CQ phosphate). A PBPK model of CQ was successfully developed to optimize dosage regimens for patients with COVID-19.

1. Introduction

Coronavirus disease 2019 (COVID-2019) which was declared a global pandemic by World Health Organization (WHO)[1], has been spreading rapidly across the world, affecting more than 200 countries and claiming more than 700,000 confirmed cases. Approximately 20% of the patients with COVID-19 experienced fatal complications, including tissue failure, septic shock, pulmonary edema, severe pneumonia, acute respiratory distress syndrome (ARDS), and mortality rate among this population was estimated to be 50%[2].

Chloroquine (CQ) was first shown to effectively suppress Severe Acute Respiratory Syndrome Coronavirus 2 (SARS-CoV-2) in *in vitro* assay[3], and has been subsequently suggested to be efficacious in slowing the deterioration of pneumonia, improving lung imaging results, decreasing viral load, and thus shorten disease duration[4,5]. CQ phosphate has been used for the treatment of malaria and autoimmune diseases for more than 70 years. According to the prescribing information, the dosage on the first day is not to exceed 1500 mg CQ phosphate, followed by daily maintenance dose of not exceeding 1000 mg CQ phosphate. Although CQ has acceptable safety profile, there are some potential safety concerns with prolonged usage, including QT prolongation, ventricular tachycardia, and retinopathy[6−9].

Studies revealed that CQ also had potential broad-spectrum antiviral activities by increasing endosomal pH being required for virus/cell fusion to accumulate in the cell, and interfering with the glycosylation of cellular receptors of SARS-CoV[10,11]. It was reported that the angiotensin-converting enzyme 2 (ACE2) receptor, which SARS-CoV-2 employs for the entry into the cell, is highly expressed in lung, gastrointestinal tract, kidney, and heart, etc., which allows SARS-CoV-2 to easily enter these organs[12]. CQ was reported to be highly and slowly accumulated in these organs[13]. Therefore, the distribution of CQ in these organs could be highly relevant to its potential effectiveness against SARS-CoV-2 and adverse events. Following the currently recommended dosing regimen for treatment of malaria or rheumatoid arthritis, it is likely that drug concentration at the site of action is exceedingly higher than the efficacious concentration (EC_{50}) needed to suppress the SARS-CoV-2 *in vitro*. Meanwhile, higher tissue accumulation of CQ may lead to adverse events. Therefore, dose of CQ should be optimized by considering exposure−efficacy and exposure−safety relationships of CQ. Among the infected patients, there are approximately 30% elderly, 30% with other complications such as hypertension and diabetes, as well as pregnant women and children (approximately 2%)[2,14,15]. Dose selection and optimization in each special population often presents as a challenge for health care providers in the clinical setting. Therefore, there is an urgent need to develop an individualized dosing strategy for each vulnerable population for the safe and effective use of CQ phosphate against SARS-CoV-2.

Physiologically-based pharmacokinetic (PBPK) model is an important mathematical tool that incorporates pharmacokinetic properties of drug and physiology, and allows the simulation of pharmacokinetic profiles of drug in plasma as well as other organs and tissues, including the site of action. It can also be used to predict drug PK in different patient populations under different treatment regimens. In Feb 2020, we employed an initial CQ PBPK model to simulate systemic and lung concentrations to support dosing recommendations of a clinical study in Wuhan (ChiCTR2000029898, ChiCTR2000029899)[16]. The initial CQ PBPK model was based on an earlier model developed by Certara UK (Simcyp Division) in collaboration with the Bill & Melinda Gates Foundation (Seattle, WA, USA) and Medicines for Malaria Venture, and is freely available within a Global Health PBPK model repository (https://members.simcyp.com/account/globalHealthRepository/). In addition, there is another report for Zika virus infection during pregnancy, where the PBPK model of chloroquine was established and validated by clinical blood and plasma time−concentration profiles[17]. Neither of the above two models reported the model construction or predictions in tissues. As the distribution of CQ in tissues could be highly relevant to its potential effectiveness against SARS-CoV-2 and adverse events, our study aims to update the initial a PBPK model of CQ to i) understand the drug exposure in various tissues under different treatment regimens of CQ phosphate, ii) use the model to predict the drug concentration at the site of action as well as in the tissues of interest where toxicity is of concern, and iii) subsequently support dose selection in different patient populations infected with SARS-CoV-2. We also reported the pharmacokinetic data of Chinese patients with COVID-19 for the first time to validate the PBPK model.

2. Methods

2.1. Data collection

The physicochemical characteristics and pharmacokinetic parameters of chloroquine were collected in Pubmed and Embase database through literature research. Among these parameters, pK_a, Log*P*, and *B*/*P* ratio were generated from *in vitro* experimental data[18]. The fractional contribution of renal elimination and CYP2C8 and CYP3A4 were derived from public results[19,20]. The permeability coefficient of chloroquine in human lung adenocarcinoma-3 (Calu-3, parameter relevant for predicting lung drug concentrations) cells was predicted by the QSAR model built in Simcyp software (Version 18, Certara, UK).

All clinical pharmacokinetic data of chloroquine were collected from Pubmed and Embase databases. The key words used for the search were "Clinical Pharmacokinetic and Chloroquine". The publications from January 1, 1940 to February 29, 2020 were reviewed. At similar dose levels and comparable patient population, the blood drug concentration of chloroquine is significantly higher or lower than the observed values of similar studies by five-fold or more would be excluded. When pharmacokinetic parameters were not available, data were obtained from the concentration−time profiles in the publications by Plot Digitizer (GetData, Version 2.26), and were applied in Phoenix (Version 8.6, Certara, UK) to calculate the corresponding main PK parameters (area under curve, AUC and maximum drug concentration, C_{max}).

2.2. Development of PBPK model

Simcyp (Version 18, Certara, UK) software was used to develop the PBPK model of CQ. The initial chloroquine PBPK model was developed by Certara UK (Simcyp Division) in collaboration with the Bill & Melinda Gates Foundation (Seattle, WA, USA) and Medicines for Malaria Venture.

A first-order absorption model with the input of f_a and k_a (fraction absorbed and first-order absorption constant, respectively) was used to describe the drug absorption process; a full-PBPK model was used to describe the drug distribution characteristics; the enzyme kinetic data and renal clearance data were used to describe the elimination characteristics; a model of permeability-rate limited mechanism was used to predict the pharmacokinetics of chloroquine in lung[21], heart, liver, and kidney tissues, and the perfusion-limited model was assumed in other organs/tissues.

Intracellular CQ accumulation[22] was characterized by the inclusion of efflux and uptake mechanisms through undefined transporters in lung permeability-rate limited tissue compartments, with passive diffusion clearance (CL_{pd}) optimized based on the ratio of time varying tissue-to-plasma concentration ratio (K_p) and the ratio of the elimination half-life of chloroquine in tissues to that of plasma (R_t) reported in rat. Because heart, liver, and kidney have high expression of ACE2, and CQ is known to cause cardiac toxicity, we established additional, separate models (compound files) of CQ each representing heart, liver, or kidney with an "user defined additional organ" to explore drug accumulation dynamics. For each of these additional models, K_p, R_t, observed in rats and reported V_{ss} in human of 137.8 L/kg were used to optimize uptake and efflux mechanisms by undefined transporters.

2.3. Validation of PBPK model

The Simcyp Simulator trial design was set to match population demographics (including ethnicity, age, and sex), as well as the dosing and blood collection time points of each literature report. Each simulation includes 10 trials with 10 subjects in each trial. Simulated AUC and C_{max} were compared with clinical observations to assess the predictive performance of the PBPK model. Evaluation criteria are: 1) the observed value is within the 90% confidence interval of the predicted value; 2) the ratio of simulated AUC and C_{max} values are within 2-fold namely, $0.5 \leq \text{ratio} \leq 2.0$ of the observed values. The use of a tighter boundary (within 25%) was also examined.

Two methods were applied to support the use of PBPK model for predicting tissue drug concentrations: 1) the ratio of time dependent K_p of CQ in rats[23] and predicted K_p in human; and 2) the ratio of the elimination half-life of CQ in R_t observed in rats[23] and predicted R_t in human by PBPK model. Evaluation criteria are: 1) overlapping of the prediction profiles in human and observation profiles in rats and comparison of the variability of K_p in rats and the predicted variability of human K_p; 2) The variation range of the calculated R_t value should be within 2-fold, namely, $0.5 \leq R_t \leq 2.0$.

2.4. Dosage regimen design and simulation

According to the preliminary clinical data from novel COVID-19 patients[5], the dosing schedule of 500 mg BID for 7 days was recommended in the Guidelines (7th edition) for the Prevention, Diagnosis, and Treatment of Pneumonia Caused by COVID-19 issued by the National Health Commission of the People's Republic of China. Assuming this dose regimen is effective, we chose to predict the trough concentration in lung tissue on the fifth day (at post-dose 120 h) as an indicator of the minimum efficacious concentration, and the predicted lung tissue $AUC_{0-120\ h}$ as the minimum efficacious exposure level. In addition, safety limits and warning limits were set based on the dose−safety relationship of CQ in the rheumatoid arthritis patients[24].

According to the approved dosage in product label, the standard antimalarial treatments (Regimen A), the highest dose that demonstrates symptom improvement in the treatment of rheumatoid arthritis (Regimen B) and the apparent effective clinical treatment (Regimen C) were selected as reference regimens. Using PBPK model, we simulated PK profiles of CQ under these reference regimens and overlaid predictions of the above efficacious and safety concentrations. These simulations guided us to propose three dosage regimens individualized for the following patients with COVID-19: acute patients (Regimen D), moderate patients (Regimen E) and special populations (Regimen F). The simulated populations include Chinese healthy volunteers, children (0−17 years old), pregnant women (in second trimester), elderly (65−98 years old) and patients with hepatic and renal impairment. Unless otherwise stated, default models within SimCYP population library were used. Ratio of male to female subjects was set to 1:1 for all simulations.

2.5. Clinical pharmacokinetic study of COVID-19 patients

An open-label, single-center study (Ethical review approval number: PJ-NBEY-KY-2020-063-01) was conducted to assess the safety, efficacy, and pharmacokinetics of CQ in patients with COVID-19. A total of eight patients weighing more than 60 kg were orally given 500 mg CQ phosphate BID for 7 days (same with Regimen C). Plasma samples on Day 1, Day 3, Day 5, Day 7 and Day 14 were collected prior to dose administration. The plasma concentrations of CQ were determined using a validated high-performance liquid chromatography−tandem mass spectrometry (HPLC−MS/MS) method (see details in Supporting Information). The study was approved by the Ethics Committee of Ningbo Hwamei Hospital, University of Chinese Academy of Sciences (Ningbo, China), and was performed in accordance with the Declaration of Helsinki. All subjects signed the Informed Consent Form (ICF) before the study.

3. Results

A PBPK model of CQ incorporating in-depth tissue distribution in the lung was developed and validated using CQ PK data from human blood and plasma, and tissue distribution informed from reported rat plasma and tissues. With this model, we can propose an appropriate dose optimization strategy to treat COVID-19 in acute patients, moderate patients, and special vulnerable populations who may need dose adjustments. The overall model-informed dosing strategy is shown in Fig. 1.

3.1. Development of PBPK model

The final model parameters and sources are shown in Table 1. A total of 28 articles related to human pharmacokinetics of chloroquine were collected based on the search criteria. There were four articles that were excluded according to the exclusion criteria, and a total of 39 CQ concentration−time profiles from different populations following administration of CQ phosphate were included (the retrieval method is shown in Supporting Information Fig. S1. Of these studies, one was used to build the model[25], and the remaining 38 profiles were used to validate the model. The population characteristics of all drug concentration−time curves and the design of dosing regimens are shown in Supporting Information Table S1.

3.2. Validation of PBPK model

The 38 concentration−time profiles from different clinical studies were compared with the predicted blood or plasma concentrations to verify the predictability of the PBPK model. The results show that 94% (31/33) of the observed AUC values were adequately described by PBPK simulations within 0.5−2.0-fold, and 45% (15/33) of observed AUC values were described by PBPK simulations within 0.8−1.25-fold. Regarding C_{max}, 97% (32/33) observed C_{max} values were described by PBPK simulations within 0.5−2.0-fold, and 18% (6/33) observed C_{max} values were described by PBPK simulations within 0.8−1.25-fold. Validation results are shown in Fig. 2, which includes data used for model building[25].

Fig. 3 shows that the overall trends of change on the PBPK simulated ratios (K_p) of tissue drug concentrations to plasma drug concentrations over 0−144 h after a single dose of CQ were similar to that observed in rats[23]. The ratio (R_t) of elimination half-life of chloroquine in tissues to elimination half-life in plasma is between 0.5 and 2.0 as listed in Table 2[23]. These evidences helped to increase the confidence in the PBPK simulated CQ exposures in lung, heart, liver and kidney.

3.3. Dosage regimen design and simulation

There are total of six regimens of CQ phosphate investigated in this study (Table 3). PBPK model was used to simulate regimens A−E in healthy Chinese subjects. Simulation of Regimen F was tested in Chinese healthy volunteers, Geriatric Northern European Caucasians (NEC), cirrhosis (mild, moderate and severe), renal glomerular filtration rate (GFR, 30−60 mL/min/1.73 cm^2 and less than 30 mL/min/1.73 cm^2), pregnancy (in second trimester) and pediatric populations default in Simcyp (Version 18.0).

The basis for dose selection is described as follows. Regimen C has been clinically used as an apparent efficacious dose[5]. The PBPK model predicted trough concentration in the lung tissue under Regimen C on Day 5 is 60.6 μg/mL, and the predicted total exposure for five consecutive days ($AUC_{0-120\ h}$) is 3020 h μg/mL. These two values are defined as the effective concentration and the effective exposure, respectively. Based on Frisk-Holmberg et al.[24], the peak serum concentration with almost no adverse reactions was 400 ng/mL, so it was used as a safety limit (similar to a no-adverse effect level). The warning limit was set at a maximum serum concentration of 800 ng/mL, at which adverse effects were observed in approximately 80% subjects. Assuming plasma concentrations are equivalent to serum concentrations, we used PBPK model to simulate plasma and lung tissue concentrations of CQ under six different regimens (Table 3). Simulated drug concentration−time curves in plasma, blood, and lung tissue are shown in Fig. 4.

The simulation results show that the predicted population mean C_{max} of the conventional clinical treatment Regimens A and B were below 400 ng/mL, which was consistent with clinical evidence for the approved indications. Regimen C mimics clinical

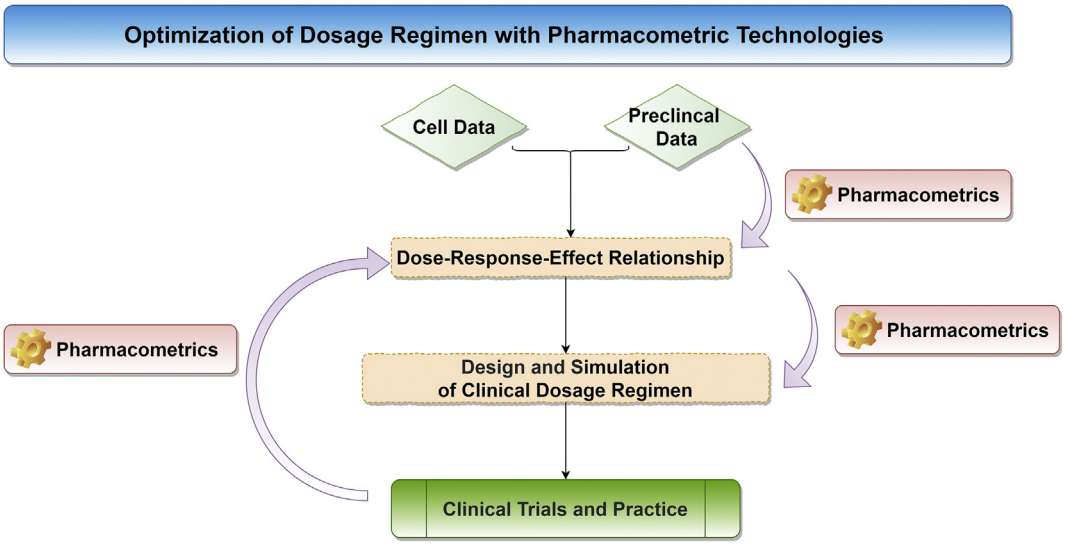

Figure 1 Overall research strategy.

Table 1 Physicochemical properties and pharmacokinetic parameters of chloroquine used for the development of the PBPK model[a].

Parameter	Input value	Source
Physicochemical properties		
Molecular weight (g/mol)	319.87	
Log*P*	4.37	Calculated from measured Log$D_{7.4}$ = 0.93[18]
Compound type	Diprotic base	
pK_a	9.94, 8.40	Measured[18]
Blood-to-plasma partition ratio	3.50	Measured[18]
Hematocrit	45.0	Assumed
Fraction unbound in plasma	0.40	Measured[33,34]
Absorption		
Absorption model	First-order	
Fraction available from dosage form (f_a)	1	Assumed
Absorption rate constant (k_a, h^{-1})	0.50	Optimized *via* sensitivity analysis for T_{max} about 4 h
Unbound fraction of drug in enterocytes (f_{uGut})	1	Assumed
Polar surface area (Å^2)	25.7	
Distribution		
Distribution model	Full PBPK model	
V_{ss} (L/kg)	137.8	Method 2 plus K_p scalar optimized to recover the observed to equal mean observed human V_{ss}[35,36]
K_p scalar	2.755	
Elimination		
Clearance type	Enzyme kinetics	
CL_{int} of recombinant CYP2C8 (μL/min/pmol of isoform)	0.269	Calculated using retrograde model with fe 0.5, fmCYP2C8 0.25, fmCYP3A4 0.15 and fm undefined 0.1[19,20,37]
CL_{int} of recombinant CYP3A4 (μL/min/pmol of isoform)	0.0283	
Additional clearance of HLM (μL/min/mg protein)	2.58	
Typical renal clearance CL_R(L/h)	20.76	
Concentration of inhibitor that supports half maximal inhibition (K_i, μmol/L) CYP2D6	3.15	
Fraction of unbound drug in the *in vitro* microsomal incubation (f_{umic})	0.797	Calculated for 0.1 mg/mL from measured value of 0.496 at 0.4 mg/mL
Permeability Ltd. organs		
Lung		Use permeability limited lung model
Log$D_{6.5}$	−0.196	Predicted by Simcyp
Number of hydrogen bond donors (HBD)	1	Drug bank
Fraction unbound in pulmonary mass	0.001	Optimized based on K_p and R_t in rat
An undefined, transporter-mediated clearance (uL/min/cm^2 for lung and uL/min 10^6 for granuloma)	0.015	
Whole organ passive diffusion clearance between intra- and extra-cellular water (L/h)	0.1	Optimized based on K_p and R_t in rat and V_{ss} = 137.8 (L/kg); user defined additional organ is permeability limited
Passive diffusion clearance for heart CL_{heart} (uL/min)	0.1	
Uptake clearance for heart CL_{heart} (uL/min)	11,000	
Efflux clearance for heart CL_{heart} (uL/min)	9	
Passive diffusion clearance for heart CL_{liver} (uL/min)	0.1	
Uptake clearance for liver CL_{liver} (uL/min)	59,000	
Efflux clearance for liver CL_{liver} (uL/min)	9	
Passive diffusion clearance for heart CL_{kidney} (uL/min)	0.1	
Uptake clearance for kidney CL_{kidney} (uL/min)	34,000	
Efflux clearance for kidney CL_{kidney} (uL/min)	10	

Abbreviations: *P*, octanol−water partition coefficient; PBPK, physiologically-based pharmacokinetic; V_{ss}, volume of distribution at steady-state; K_p, partition coefficient; HLM, human liver microsome.

[a]Rodgers and Rowland prediction method was used.

study in which apparent efficacy in COVID-19 patients was observed[5]. Under this regimen, the model simulated population mean C_{max} of plasma exceeded 400 ng/mL, but was substantially below 800 ng/mL.

Regimen D was designed for treating patients with acute COVID-19. Under this regimen, the model-simulated population mean trough concentration in lung tissue could reach 60.6 μg/mL in 3−5 days. Regimen E was designed for treating moderate COVID-19 infected patients, and model simulated mean trough concentration in lung tissue can reach 60.6 μg/mL in 5−7 days. The total exposures ($AUC_{0-120\ h}$) for five consecutive days of both Regimens D and E (3650 and 3220 h μg/mL, respectively) are greater than 3020 h μg/mL. The total exposures ($AUC_{0-240\ h}$) for 10 consecutive days of Regimens F (6470 h μg/mL) is about twice as much as 3020 h μg/mL. When the simulated concentration−time profile is extended to 28 days, the results shows that the elimination of the drug in the body is slow and drug accumulation in the tissues is high. For example, in Regimen C,

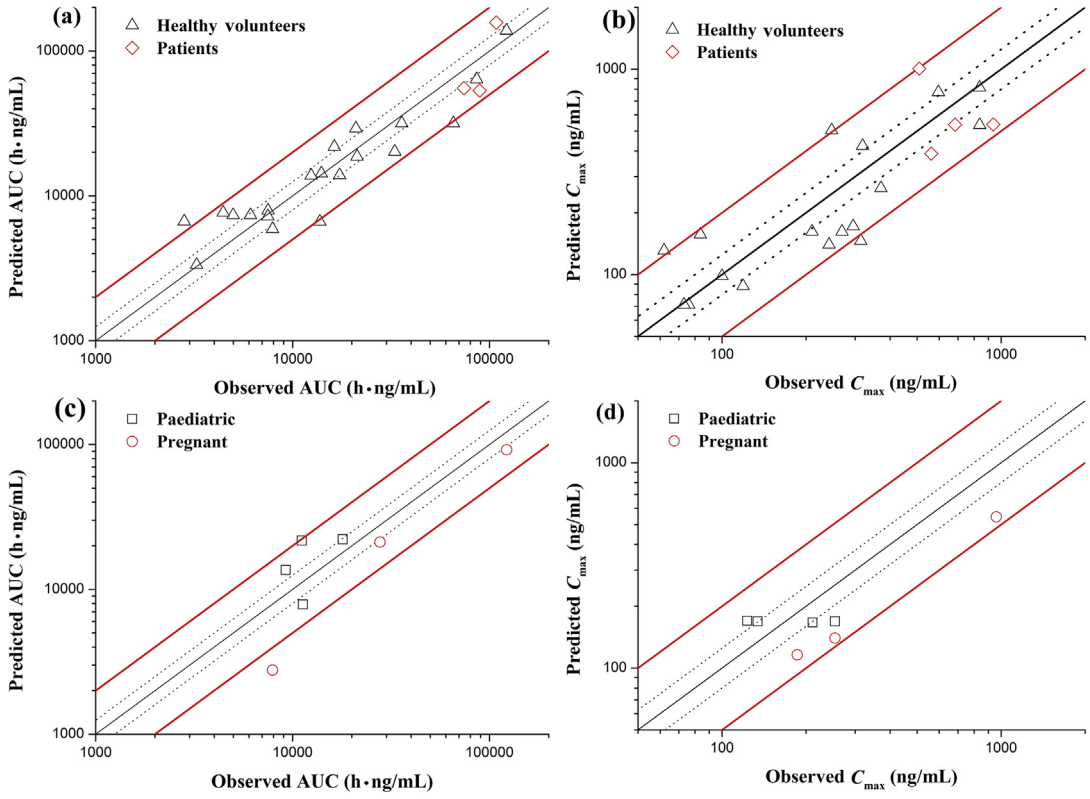

Figure 2 Validation results of plasma and blood concentrations of PBPK model. (a) AUC for healthy subjects and patients; (b) C_{max} for healthy subjects and patients; (c) AUC for pregnant and pediatric; (d) C_{max} for pregnant and pediatric.

plasma concentration on Day 28 reached 60.4 ng/mL, whereas predicted lung tissue concentration was 124 μg/mL. Simulations under these regimens also indicate high CQ concentrations in the heart, liver, and kidneys (Fig. 5, take Regimen F for example).

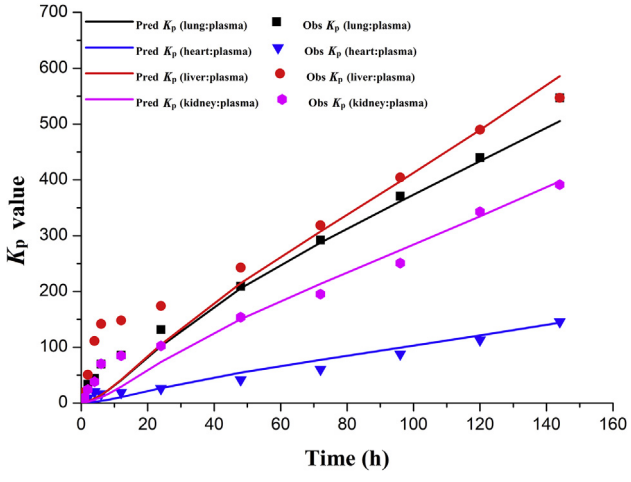

Figure 3 Time dependent tissue concentrations of PBPK model (K_p: the ratio of plasma drug concentration to tissue drug concentration).

Regimen F was a reduced-dose regimen intended for other vulnerable populations with COVID-19. In these populations, exposure may be increased due to reduced drug elimination. Model simulated results show that CQ exposure in the elderly (65−98 years), and patients with hepatic and renal impairment were higher than in normal adults, but the exposure in pregnant women was lower as shown in Fig. 6. The results showing that children of different age groups could achieve similar plasma and blood exposure to adults by adjusting the dose regimen are shown in Fig. 7.

3.4. *Clinical pharmacokinetic study of COVID-19 patients*

A total of 25 plasma samples were collected and analyzed successfully from eight patients with moderate COVID-19. After multiple oral doses (500 mg BID, CQ phosphate) for 7 days, the mean concentrations were 169.4 ± 106.4, 322.1 ± 112.0, 245.4 ± 89.2, and 159.5 ± 93.1 ng/mL for Day 3, Day 5, Day 7, and Day 14, respectively. In accordance with this protocol, we compared the PBPK-model-predicted CQ concentrations in healthy Chinese volunteers to these observed data in patients with COVID-19, as shown in Fig. 8, and the results show that the predicted mean concentration was within 2-fold of the observed mean concentration, indicating that the pathological state might have little influence on the pharmacokinetic characteristics of drug in plasma.

Table 2 Comparison of human predicted R_t with observes R_t in rats.

Item	Lung					Heart	Liver	Kidney
	Right top lobe	Right middle lobe	Right low lobe	Left top lobe	Left low lobe			
Tissue half-life (day)	29.7	38.1	22.2	25.2	22.2	24.5	33.0	25.0
Predicted ratio in human	3.79	4.86	2.83	3.21	2.84	3.13	4.22	3.19
Obvious ratio in rat	4.89	4.89	4.89	4.89	4.89	3.56	2.90	3.34
Ratio	0.77	0.99	0.58	0.66	0.58	0.88	1.46	0.96

Abbreviations: R_t ratio of tissue half-life to plasma half-life.

Table 3 Predicted plasma and lung tissue exposure under different dosage regimens of chloroquine phosphate.

No.	Dosage design	Visual population (default models in Simcyp)	Plasma	Lung (mean value of five lobes)								
			C_{max} (ng/mL)	AUC (h·μg/mL)		C_{trough} (μg/mL)					AUC (h·μg/mL)	
				0 −120 h	0 −240 h	Day 1 (24 h)	Day 3 (72 h)	Day 5 (120 h)	Day 7 (168 h)	Day 10 (240 h)	0 −120 h	0 −240 h
A	Day 1: 1000 mg, 500 mg Days 2−3: 500 mg QD	Chinese healthy volunteers	215	17.3	27.4	10.5	29.0	39.4	45.9	51.2	2760	8350
B	Days 1−10: 500 mg QD	Chinese healthy volunteers	283	13.6	38.7	3.79	16.0	32.0	50.6	81.1	1690	8450
C	Days 1−7: 500 mg BID	Chinese healthy volunteers	416	25.5	63.1	6.21	29.2	60.6	97.2	129	3020	15,100
D	Day 1: 750 mg BID Days 2−5: 500 mg BID	Chinese healthy volunteers	364	29.2	54.9	9.32	35.6	68.8	90.2	108	3650	14,700
E	Day 1: 750 mg, 500 mg Days 2−3: 500 mg BID Days 4−5: 250 mg BID	Chinese healthy volunteers	270	23.9	43.1	8.65	32.8	56.7	71.8	84.1	3220	12,000
F	Days 1−5: 250 mg BID	Chinese healthy volunteers	172	12.5	24.4	3.11	14.6	30.3	40.4	48.6	1510	6470

4. Discussion

4.1. *Dose optimization strategy for outbreak of COVID-19*

At present, in many clinical studies (ChiCTR2000029939, ChiCTR2000029935, ChiCTR2000029899, etc.) conducted in China, there are no standard recommended dosing regimens of chloroquine phosphate (see Supporting Information Table S2). After preliminary clinical research and exploration, National Health Commission of the People's Republic of China proposed that the recommended dose of chloroquine phosphate for the treatment of COVID-19 was 500 mg BID for adults (18−65 years), and continuous administration should not exceed 7 days. In clinical setting, the dose is often being adjusted case-by-case based on the experience of the clinicians, and the selection of optimal dosing regimen would require a well-designed clinical trial with prolonged time period for safety monitoring with large sample size. Under the current urgent need of the treatment to help patients with COVID-19, it is not feasible to conduct such conventional clinical trials to optimize dose selection for CQ. Therefore, we borrowed the principles of the US FDA's Animal Rule[26] and used PBPK modeling as a tool to combine the available cell-level and animal-level data and describe quantitatively the dose−exposure−response relationships of CQ. Modeling and simulation approach were employed to understand and translate the kinetics of CQ from the cell level to the whole-body level, and were used to support the design of dosing regimens for different patient populations.

4.2. *Advantages of the updated PBPK model*

PBPK model integrates a series of mathematical equations that describe human physiological and biochemical pathways, drug physicochemical properties and drug mechanistic pharmacokinetic data parameters to systematically study the body's effects on drugs[27]. The model-based selection of dosing regimens of CQ presented in our study was based on the following knowledge: *in vitro* antiviral potency[3], historical knowledge of exposure−response relationship for safety[24], apparent efficacy reported recently (*e.g.*, under dosing Regimen C)[5], and a PBPK model capable of predicting drug concentrations in plasma, blood, and tissues. The novelty of this study includes (i) mimicking the physiological characteristics of time-dependent accumulation through an active transport mechanism in the model, which reasonably captured high accumulation of chloroquine in the cells[22] for better prediction of the local PK characteristics of CQ

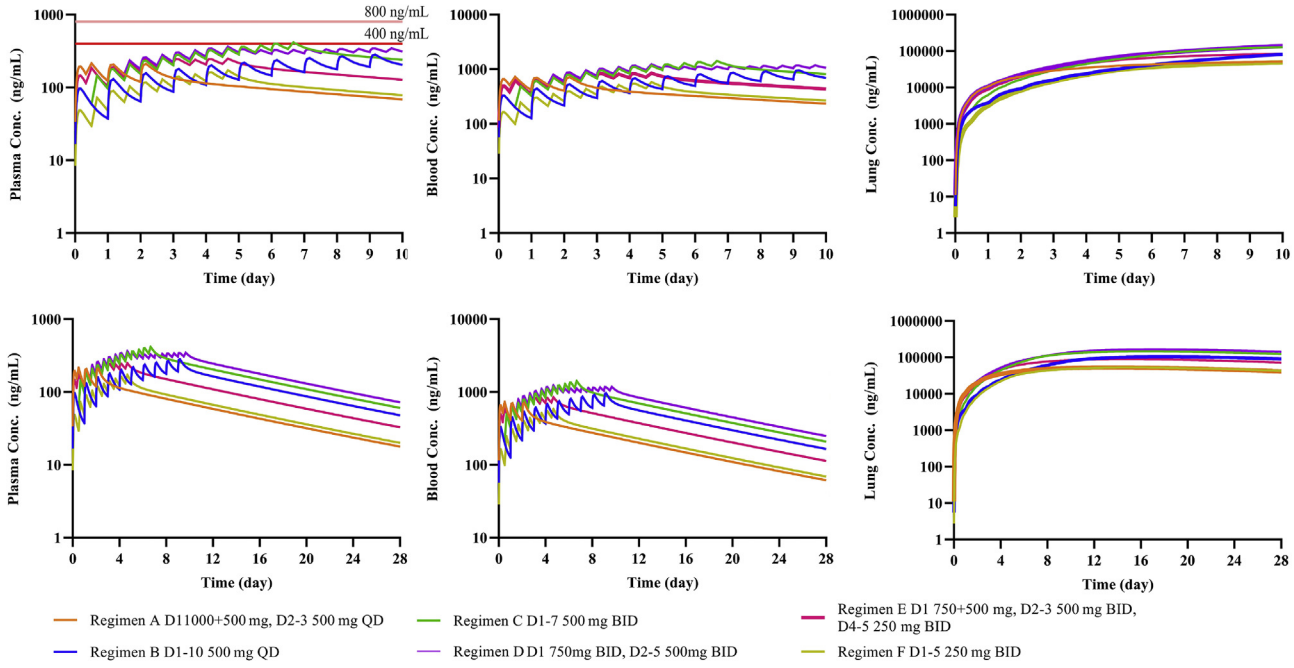

Figure 4 Simulation results of six dosage regimens. (a) Plasma concentration for 10 days; (b) plasma concentration for 28 days; (c) blood concentration for 10 days; (d) blood concentration for 28 days; (e) lung concentration for 10 days; (f): lung concentration for 28 days. Additional models (SimCYP compound files) for heart, liver, or kidneys, respectively, were used to simulate tissue concentrations (See Methods).

in permeability-limited tissues, and (ii) supporting PBPK prediction of human tissue drug concentrations using animal data. The collection of the lung tissue sample presents a challenge in clinical operation. Considering that the accumulation of CQ in tissues was mainly due to passive diffusion and increased intracellular pH, we assumed that there is minimal inter-species difference. It is thus reasonable to use the rat K_p and R_t values to support the prediction of tissue concentrations using PBPK models. In the absence of clinical experimental data, this is a powerful alternative to predict the high K_p ratios of human according to observations in rats.

As ACE2 receptor is highly expressed in liver, kidney, and heart, which allows SARS-CoV-2 virus to easily enter these

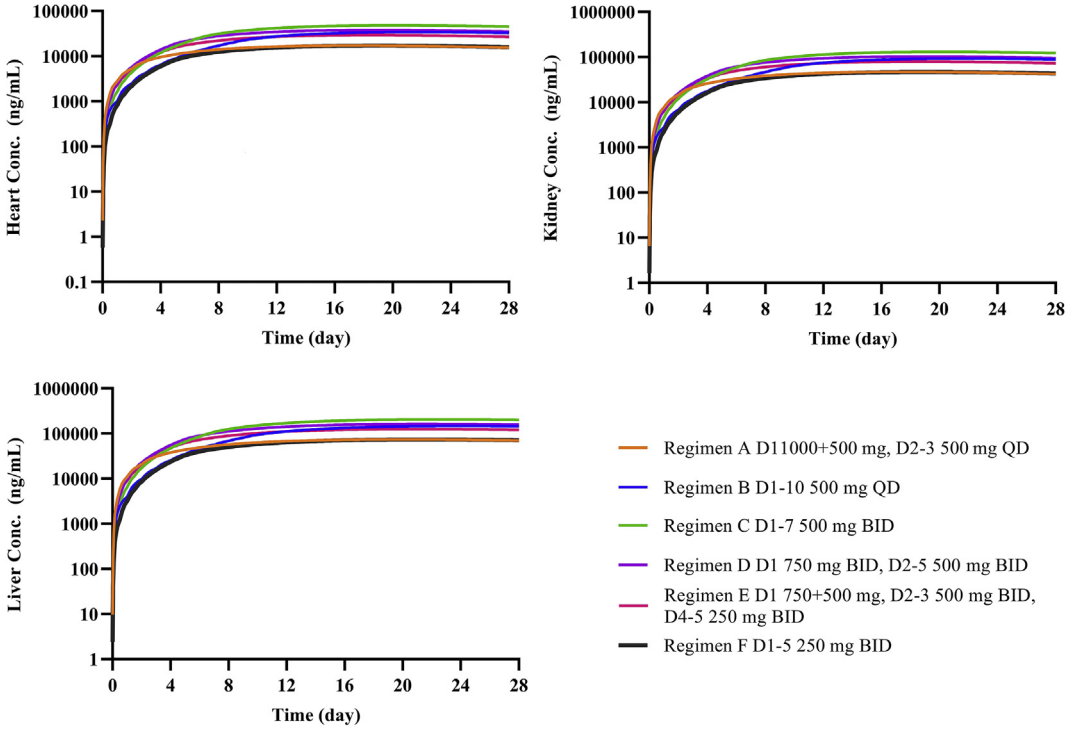

Figure 5 Simulation results of six dosage regimens. (a) Heart concentration for 28 days; (b) liver concentration for 28 days; (c) kidney concentration for 28 days.

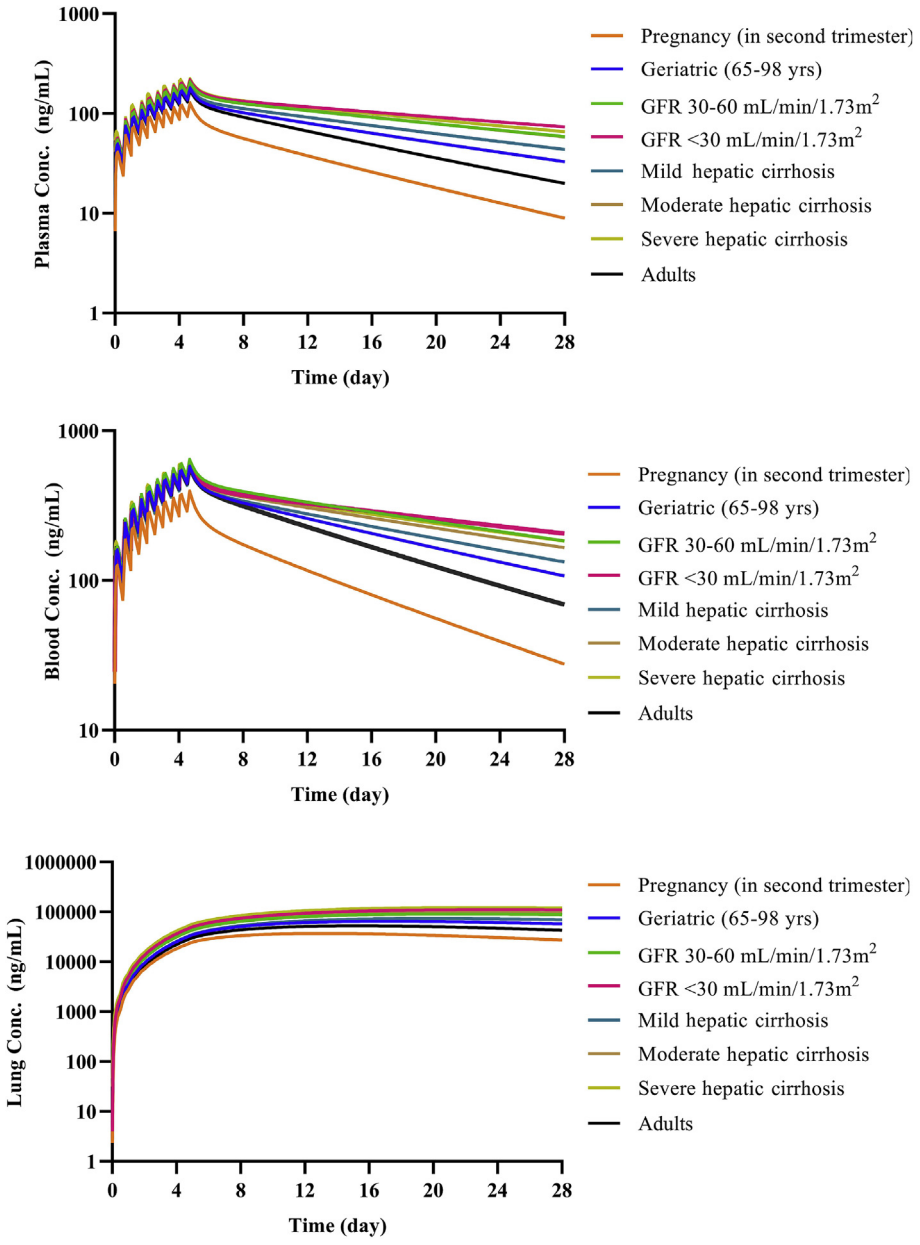

Figure 6 Simulation results of special populations with Regimen F. (a) Plasma concentration for 28 days; (b) blood concentration for 28 days; (c) lung concentration for 28 days.

organs[28], accumulation of CQ in these organs could be highly relevant to its potential effectiveness. Meanwhile, significant drug accumulation in these organs may raise safety concerns. Considering it could passively enter tissue cells and can be trapped in some organelles in the ionized form[22], permeability-limited distribution was assumed in these tissues to characterize the time-dependent cellular drug accumulation. The simulated results showed that CQ could retain in tissues for a long time after dosing stopped.

4.3. Considerations of dosing regimen for special population

In order to apply right dosing regimen to special populations, we performed model simulations to assess the relationship of drug exposure and safety. The liver metabolic enzyme activity and glomerular filtration rate of CQ in these special populations are altered[29–32]. However, as CQ was almost equally eliminated by CYP450-mediated metabolism and renal secretion[13], dramatic change in either pathway theoretically might not lead to significant increase in CQ exposure, as shown by our simulation results. The results suggested that there is no drastic increase in exposure for the elderly, patients with renal or hepatic impaired functions, or pregnant women. In these subjects, dose adjustment can be used according to proposed regimens based on exposure-matching. Considering known safety and emerging information on efficacy, we proposed the use of Regimen F as starting regimen for treating COVID-19 in these special populations. However, in other sensitive populations, such as children with different ages or the patients with both of impaired renal and hepatic functions, CQ exposure may increase dramatically, and CQ should be avoided or

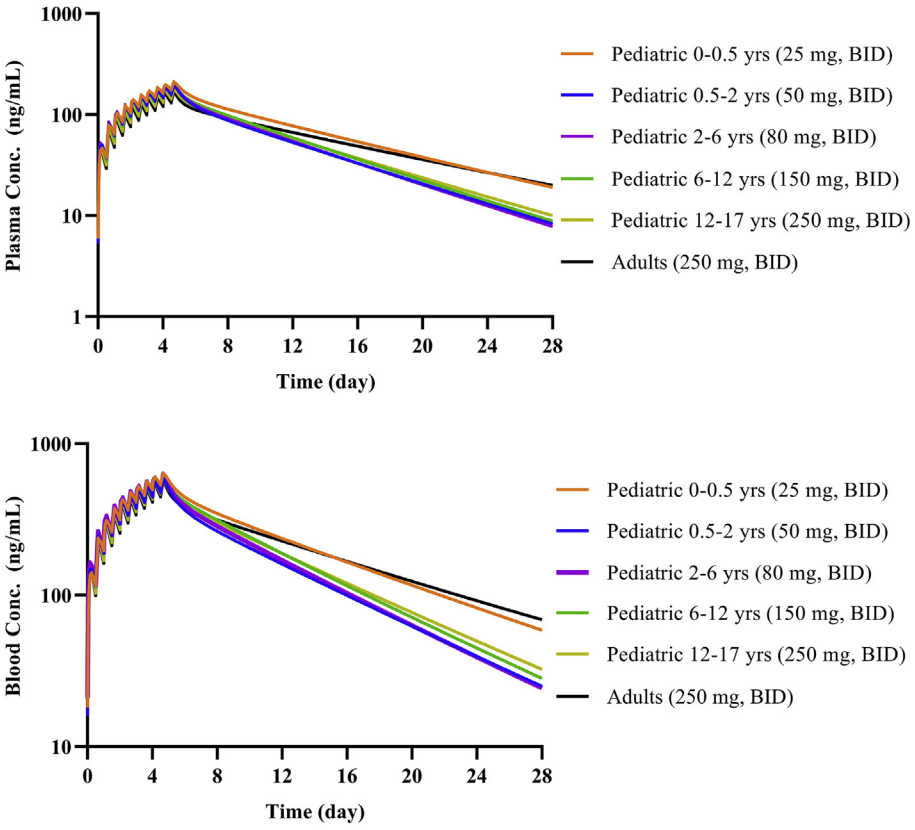

Figure 7 Simulation results of children with Regimen F. (a) Plasma concentration for 28 days; (b) blood concentration for 28 days.

used very cautiously if it has to be used. For example, a regimen with a lower loading dose and less frequent dosing may be considered. The developed drug model and population models can be used to predict the exposure and design different dosage regimens. Linking the exposure with clinical effect, the dose of CQ in special population can be properly guided.

4.4. Limitations of the research

Multiple assumptions were made in this study and several limitations warrant additional research to further enhance the predictability of the model. First, we assumed same underlying physiology between healthy subjects, patients with acute or moderate COVID-19 and virtual populations that better represent COVID-19 disease related pathophysiology may be needed. For example, although simulated mean CQ concentrations were within 2-fold of the observed concentrations, observed results are highly variable, and simulated mean concentration appears to underestimate and overestimate observed values on Day 4 and Day 6, respectively (Fig. 8). Disease progression during intervention of CQ may affect the PK of the drug. Sensitivity analysis was performed on the newly established model, such as the change of free fraction of CQ in lung tissue, pulmonary blood flow, pulmonary pH, and intrinsic clearance rate (CL_{int}) of lung tissue. The results suggest that these physiological and pathological changes had little impact on the predictions (data not shown). Second, simulations were conducted in various virtual populations that have been developed based on Caucasian data. The predictability of CQ pharmacokinetics in vulnerable populations may require further validation. Third, we focused on liver, lung, heart, and kidney when parameterizing permeability-limited drug distribution. Future research is needed to characterize drug distribution to other organs such as the eyes. CQ is known to cause retinopathy, understanding tissue distribution in this organ is important. In addition, several assumptions were made when parameterizing permeability-limited CQ distribution, including the use of apparent active transport mechanism to capture time-dependent drug accumulation, the use of animal data to support prediction of tissue concentrations in humans, and the use of additional models and undefined extra organ to describe permeability-limited tissue distribution in the heart, liver, and kidney. Last but not the

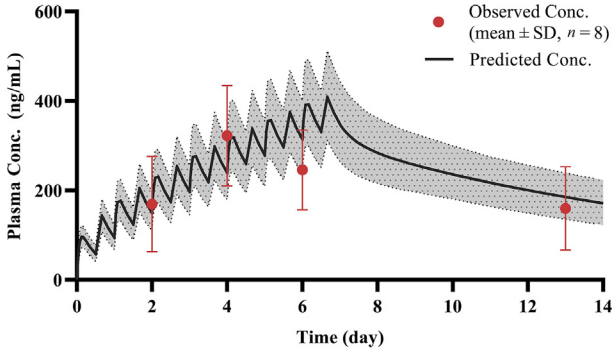

Figure 8 Simulated plasma concentration time profiles of CQ in Chinese healthy subjects overlaid with observed plasma concentration time profiles of CQ in Chinese COVID-19 patients (500 mg BID for 7 days, CQ phosphate). Solid lines represent mean simulated concentration time profile with dotted lines representing 5th and 95th percentile range. Red circles represent observed clinical data from COVID-19 study. Where presented, error bars indicate standard deviation, $n = 8$.

least, it has to be noted that discussion on exposure-efficacy relationship discussed in this manuscript is exploratory as several assumptions were used. In general, the concentration of free plasma should be compared with EC_{50}. Considering the high accumulation of this drug in cells, it should be valuable to compare intracellular EC_{50} with lung tissue concentration. In *in vitro* experiment[16], we observed time-dependent decrease in EC_{50} values, and intracellular drug accumulation over time may be one of the causes (*e.g.,* higher concentration after longer incubation). This may be modified when we can truly measure intracellular CQ concentrations *in vitro* and *in vivo* and then compare intracellular EC_{50} with lung tissue concentration. We explored the use of *in vivo* efficacious concentration with assumption that anti-viral outcome from a recommended dosage regimen for COVID-19, which should be further confirmed by a strict randomized and well-controlled trail. If the regimen of 5th day of 500 mg BID confirmed to be modified, then the final plan also needs to be optimized, but the strategy is similar.

5. Conclusions

We proposed a model-informed dose selection strategy under emergency situation. First, we established and validated a novel PBPK model to predict concentrations in lung, heart, liver and kidney assuming permeability-limited distribution by mimicking the physiological characteristics of time-dependent accumulation through an active transport mechanism in the model. Second, we selected the simulated lung trough concentration on Day 5 and $AUC_{0-120\,h}$ in patients with a dose of 500 mg BID (CQ phosphate) as effective target and selected 800 ng/mL of plasma trough concentration as safety limit according to reported clinical exposure−response relationship. Third, we optimized different dosing regimens for different type of patients using PBPK model. Fourth, pharmacokinetic data from Chinese patients with moderate COVID-19 was firstly reported and employed to validate the model. Recognizing the limitations and assumptions, we are presenting a mechanism-based, rationalized modeling approach to healthcare providers to facilitate their decisions on dose selection. We hope our PBPK model could be applied for optimizing the use of CQ for treatment of COVID-19, and our dosing optimizing strategy could help accelerate safe and effective use of other anti-COVID-19 drugs.

Acknowledgements

We thank Drs. Eleanor Howgate and Maurice Dickins for the development of the original chloroquine PBPK base model, and thank Lisa Almond, Alice Ke and Mian Zhang for providing the initial model and constructive discussions. We thank Dr. Ping Zhao, Dr. Gaohua Lu and Dr. Hoi-Kei Lon for the scientific suggestion and proofreading. This work was supported by the "13th Five-Year" National Science and Technology Major Project (grant Nos. 2017ZX09101001-002-001 and 2017ZX09304012, China) and Bill & Melinda Gates Foundation (OPP1204780, USA).

Author contributions

Dongyang Liu conceived and designed research; Haiyan Li direct the whole project; Shun Zhang designed the pharmacokinetic study; Cheng Cui, Miao Zhang and Xueting Yao developed and optimized the tissue models; Siqi Tu, Zhe Hou, and Valerie Sia Jie En performed data collection and model *in vitro*; Jing Lin and Ting Cai assayed the pharmacokinetic data. Xiaoqiang Xiang, Ning Shen, Chunli Song and Jie Qiao provided valuable suggestions; Cheng Cui wrote the paper.

Conflicts of interest

The authors declare no conflicts of interest.

Appendix A. Supporting information

Supporting data related to this article can be found at https://doi.org/10.1016/j.apsb.2020.04.007.

References

1. Sohrabi C, Alsafi Z, O'Neill N, Khan M, Kerwan A, Al-Jabir A, et al. World Health Organization declares global emergency: a review of the 2019 novel coronavirus (COVID-19). *Int J Surg* 2020;**76**:71−6.
2. Novel Coronavirus Pneumonia Emergency Response Epidemiology Team. The epidemiological characteristics of an outbreak of 2019 novel coronavirus diseases (COVID-19) in China. *Zhonghua Liuxingbingxue Zazhi* 2020;**41**:145−51.
3. Wang M, Cao R, Zhang L, Yang X, Liu J, Xu M, et al. Remdesivir and chloroquine effectively inhibit the recently emerged novel coronavirus (2019-nCoV) *in vitro*. *Cell Res* 2020;**30**:269−71.
4. Colson P, Rolain JM, Raoult D. Chloroquine for the 2019 novel coronavirus SARS-CoV-2. *Int J Antimicrob Agents* 2020;**55**:105923.
5. Gao J, Tian Z, Yang X. Breakthrough: chloroquine phosphate has shown apparent efficacy in treatment of COVID-19 associated pneumonia in clinical studies. *BioSci Trends* 2020;**14**:72−3.
6. Bernstein H, Zvaifler N, Rubin M, Mansour AM. The ocular deposition of chloroquine. *Invest Ophthalmol* 1963;**2**:384−92.
7. Haeusler IL, Chan X, Guérin PJ, White NJ. The arrhythmogenic cardiotoxicity of the quinoline and structurally related antimalarial drugs: a systematic review. *BMC Med* 2018;**16**:200.
8. Leecharoen S, Wangkaew S, Louthrenoo W. Ocular side effects of chloroquine in patients with rheumatoid arthritis, systemic lupus erythematosus and scleroderma. *J Med Assoc Thai* 2007;**90**:52−8.
9. Puavilai S, Kunavisarut S, Vatanasuk M, Timpatanapong P, Sriwong ST, Janwitayanujit S, et al. Ocular toxicity of chloroquine among Thai patients. *Int J Dermatol* 1999;**38**:934−7.
10. Willmann S, Höhn K, Edginton A, Sevestre M, Solodenko J, Weiss W, et al. Development of a physiology-based whole-body population model for assessing the influence of individual variability on the pharmacokinetics of drugs. *J Pharmacokinet Pharmacodyn* 2007;**34**:401−31.
11. Yan Y, Zou Z, Sun Y, Li X, Xu KF, Wei Y, et al. Anti-malaria drug chloroquine is highly effective in treating avian influenza A H5N1 virus infection in an animal model. *Cell Res* 2013;**23**:300−2.
12. Hamming I, Timens W, Bulthuis ML, Lely AT, Navis G, van Goor H. Tissue distribution of ACE2 protein, the functional receptor for SARS coronavirus. A first step in understanding SARS pathogenesis. *J Pathol* 2004;**203**:631−7.
13. Ducharme J, Farinotti R. Clinical pharmacokinetics and metabolism of chloroquine. Focus on recent advancements. *Clin Pharmacokinet* 1996;**31**:257−74.
14. Wu YC, Chen CS, Chan YJ. The outbreak of COVID-19: an overview. *J Chin Med Assoc* 2020;**83**:217−20.
15. Liang H, Acharya G. Novel corona virus disease (COVID-19) in pregnancy: what clinical recommendations to follow. *Acta Obstet Gynecol Scand* 2020;**99**:439−42.
16. Yao X, Ye F, Zhang M, Cui C, Huang B, Niu P, et al. *In vitro* antiviral activity and projection of optimized dosing design of hydroxychloroquine for the treatment of severe acute respiratory syndrome coronavirus 2 (SARS-CoV-2). *Clin Infect Dis* 2020. Available from: https://doi.org/10.1093/cid/ciaa237.

17. Olafuyi O, Badhan R. Dose optimization of chloroquine by pharmacokinetic modeling during pregnancy for the treatment of Zika virus infection. *J Pharm Sci* 2019;**108**:661−73.
18. Charman SA, Andreu A, Barker H, Blundell S, Campbell A, Campbell M, et al. An *in vitro* toolbox to accelerate anti-malarial drug discovery and development. *Malar J* 2020;**19**:1.
19. Projean D, Baune B, Farinotti R, Flinois JP, Beaune P, Taburet AM, et al. *In vitro* metabolism of chloroquine: identification of CYP2C8, CYP3A4, and CYP2D6 as the main isoforms catalyzing *N*-desethylchloroquine formation. *Drug Metab Dispos* 2003;**31**:748−54.
20. Kim KA, Park JY, Lee JS, Lim S. Cytochrome P450 2C8 and CYP3A4/5 are involved in chloroquine metabolism in human liver microsomes. *Arch Pharm Res* 2003;**26**:631−7.
21. Gaohua L, Wedagedera J, Small BG, Almond L, Romero K, Hermann D, et al. Development of a multicompartment permeability-limited lung PBPK model and its application in predicting pulmonary pharmacokinetics of antituberculosis drugs. *CPT Pharmacometrics Syst Pharmacol* 2015;**4**:605−13.
22. Rainsford KD, Parke AL, Clifford-Rashotte M, Kean WF. Therapy and pharmacological properties of hydroxychloroquine and chloroquine in treatment of systemic lupus erythematosus, rheumatoid arthritis and related diseases. *Inflammopharmacology* 2015;**23**:231−69.
23. Adelusi SA, Salako LA. Kinetics of the distribution and elimination of chloroquine in the rat. *Gen Pharmacol* 1982;**13**:433−7.
24. Frisk-Holmberg M, Bergkvist Y, Domeij-Nyberg B, Hellström L, Jansson F. Chloroquine serum concentration and side effects: evidence for dose-dependent kinetics. *Clin Pharmacol Ther* 1979;**25**:345−50.
25. Gustafsson LL, Walker O, Alván G, Beermann B, Estevez F, Gleisner L, et al. Disposition of chloroquine in man after single intravenous and oral doses. *Br J Clin Pharmacol* 1983;**15**:471−9.
26. Bergman KL. The animal rule: the role of clinical pharmacology in determining an effective dose in humans. *Clin Pharmacol Ther* 2015;**98**:365−8.
27. Sinha V, Zhao P, Huang SM, Zineh I. Physiologically based pharmacokinetic modeling: from regulatory science to regulatory policy. *Clin Pharmacol Ther* 2014;**95**:478−80.
28. Hoffmann M, Kleine-Weber H, Schroeder S, Krüger N, Herrler T, Erichsen S, et al. SARS-CoV-2 cell entry depends on ACE2 and TMPRSS2 and is blocked by a clinically proven protease inhibitor. *Cell* 2020;**181**:271−80.
29. Soma-Pillay P, Nelson-Piercy C, Tolppanen H, Mebazaa A. Physiological changes in pregnancy. *Cardiovasc J Afr* 2016;**27**:89−94.
30. Jeong H. Altered drug metabolism during pregnancy: hormonal regulation of drug-metabolizing enzymes. *Expet Opin Drug Metabol Toxicol* 2010;**6**:689−99.
31. Hunt CM, Westerkam WR, Stave GM, Wilson JA. Hepatic cytochrome P-4503A (CYP3A) activity in the elderly. *Mech Ageing Dev* 1992;**64**:189−99.
32. McLachlan MS. The ageing kidney. *Lancet* 1978;**2**:143−5.
33. Ofori-Adjei D, Ericsson O, Lindström B, Sjöqvist F. Protein binding of chloroquine enantiomers and desethylchloroquine. *Br J Clin Pharmacol* 1986;**22**:356−8.
34. Walker O, Birkett DJ, Alván G, Gustafsson LL, Sjöqvist F. Characterization of chloroquine plasma protein binding in man. *Br J Clin Pharmacol* 1983;**15**:375−7.
35. Edwards G, Looareesuwan S, Davies AJ, Wattanagoon Y, Phillips RE, Warrell DA. Pharmacokinetics of chloroquine in Thais: plasma and red-cell concentrations following an intravenous infusion to healthy subjects and patients with *Plasmodium vivax* malaria. *Br J Clin Pharmacol* 1988;**25**:477−85.
36. Ofori-Adjei D, Ericsson O, Lindström B, Hermansson J, Adjepon-Yamoah K, Sjöqvist F. Enantioselective analysis of chloroquine and desethylchloroquine after oral administration of racemic chloroquine. *Ther Drug Monit* 1986;**8**:457−61.
37. Walker O, Salako LA, Alván G, Ericsson O, Sjöqvist F. The disposition of chloroquine in healthy Nigerians after single intravenous and oral doses. *Br J Clin Pharmacol* 1987;**23**:295−301.